

# Amplification of Angular Rotations Using Weak Measurements

Omar S. Magaña-Loaiza,<sup>1,\*</sup> Mohammad Mirhosseini,<sup>1,†</sup> Brandon Rodenburg,<sup>1,‡</sup> and Robert W. Boyd<sup>1,2</sup>

<sup>1</sup>The Institute of Optics, University of Rochester, Rochester, New York 14627, USA

<sup>2</sup>Department of Physics, University of Ottawa, Ottawa ON K1N 6N5, Canada

We present a weak measurement protocol that permits a sensitive estimation of angular rotations based on the concept of weak-value amplification. The shift in the state of a pointer, in both angular position and the conjugate orbital angular momentum bases, is used to estimate angular rotations. This is done by an amplification of both the real and imaginary parts of the weak-value of a polarization operator that has been coupled to the pointer, which is a spatial mode, via a spin-orbit coupling. Our experiment demonstrates the first realization of weak-value amplification in the azimuthal degree of freedom. We have achieved effective amplification factors as large as 100, providing a sensitivity that is on par with more complicated methods that employ quantum states of light or extremely large values of orbital angular momentum.

PACS numbers: 03.65.Ta, 42.50.Tx, 42.50.Ex, 42.25.Hz

In 1988 Aharonov *et al.* [1] introduced a general form of quantum measurement, known as a weak measurement. In weak measurements, information is gained by weakly probing the system, while approximately preserving its initial state. The uncertainty in each measurement is large due to the weak perturbative nature of the information extraction; however, this is generally overcome by averaging over a large number of identically prepared states. The process of post-selecting the prepared system makes weak measurements interesting. Under certain conditions the outcome, which is called a weak value (WV), is not an eigenvalue of the measurement operator. In fact, WVs can even exceed the eigenvalue range of a typical strong or projective measurement and in general are complex. These features have allowed a wide range of applicability in classical and quantum contexts. For example, they have resulted in the measurement via amplification of small transverse [2, 3] and longitudinal [4–6] shifts, the direct measurement of the quantum wave function [7–9], the development of tomographic techniques [10], the amplification of optical nonlinearities [11], and the clarification of controversial debates in quantum physics [12, 13].

Recently, there has been a strong impetus to employ weak-value amplification (WVA) as an effective tool in metrology [4, 5, 14, 15]. A WVA protocol involves the preparation of an ensemble of particles with two independent degrees of freedom (DoF). These two DoFs are then coupled by means of a weak perturbation and post-selected to collapse one of the DoF, typically called the probe. Due to the coupling existing between the probe and the other DoF, called the pointer, the post-selection induces a shift in the linear position of the pointer which is proportional to the weakly induced perturbation and the WV. This has allowed the use of WVA to estimate small quantities with sensitivities comparable to quantum-enhanced metrology [4, 5, 14–16], due to the fact that the use of quantum protocols does not guarantee sensitivities beyond the standard quantum limit,

which is the limit for classical protocols [17, 18].

Besides the extensive work on the estimation of longitudinal displacements [4–6, 14, 17–19], high sensitivity measurement of angular displacements has been another topic of interest. Historically, inquiries regarding relativistic dynamics stimulated interest on the azimuthal DoF [20]. A remarkable example is the Sagnac effect. Atomic versions of the Sagnac interferometer have led to sensitive gyroscopes that permit a precise measurement of rotations [21, 22]. In addition, the use of light endowed with orbital angular momentum (OAM) has motivated interest in new forms of rotations. As identified by Allen *et al.* [23], an optical beam with azimuthal phase dependence of the form  $e^{i\ell\phi}$  carries OAM, where  $\phi$  is the azimuthal angle and  $\ell$  is the OAM value. These beams have been used for rotational control of microscopic systems [24], and exploration of effects such as the rotational Doppler shift [25] which has been recently used in techniques for detecting spinning objects [26, 27]. Recent efforts to increase the sensitivity in the measurement of angular rotations involve the generation of large values of OAM [28], quantum entanglement of high OAM values [29], or the use of N00N states in the OAM bases [30]. These protocols require complicated schemes to generate and measure photons in such exotic states. However, the concepts behind them constitute valuable resources not only for optical metrology, remote sensing, biological imaging or navigation systems [26, 27, 31], but also for the understanding of light-matter interactions [32–34].

In this work, we describe WVA in the azimuthal DoF and the processes that give rise to these effects. The first observation of these kinds of WVs suggests interesting physics from the fundamental and applied perspective. For instance, the spin-orbit coupling in our experiment gives rise to an interesting optical effect in which the perturbation of polarization induces a shift in the angular position and OAM spectrum of the pointer. We show that the real and the imaginary part of the WV for the polarization operator can be accessed by measuring the

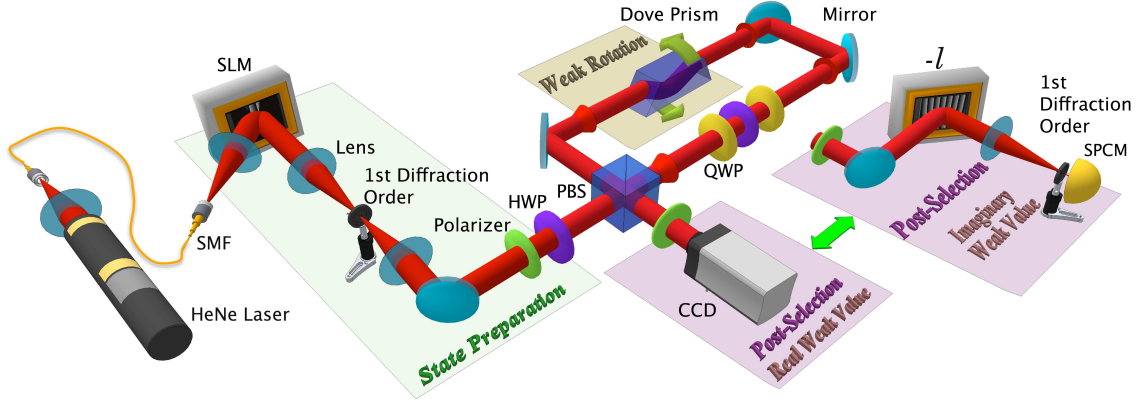


FIG. 1: Experimental Setup. A light beam from HeNe laser working at 632.8 nm is coupled into a single-mode fiber (SMF) and the output is then collimated. The beam is sent to a phase-only spatial light modulator (SLM) and then to a 4f optical system containing a spatial filter in the Fourier plane. A polarization state is prepared by means of a polarizer and a half-wave plate (HWP). A dove prism (DP), a HWP and two quarter-wave plates (QWP) are placed inside the Sagnac interferometer. The DP induces a small rotation between the counter-propagating beams; this is the weak perturbation. The QWPs together with the HWP induce a geometric phase between the H and V polarized beams. After post-selection, measurements of angular rotations and OAM spectra are performed to access the real or imaginary part of the weak-value.

angular position and its conjugate variable of OAM, respectively. Using this new form of WVs based on spin-orbit coupling, we propose a scheme for the measurement of small rotations. We demonstrate an amplification in the measurement of angular rotations that is as large as 100. The simplicity of our scheme, namely lack of need for exotic quantum state of lights or extremely large values of OAM, makes this technique potentially attractive for applications in optical metrology, remote sensing and optical manipulation of microscopic systems.

Consider the experimental setup depicted in Fig. 1. This scheme comprises three parts: state preparation, a weak perturbation, and post-selection. The state preparation involves the generation of a light beam with diagonal polarization and a well-defined spatial profile. We select the initial polarization state using a polarizer and a half-wave plate (HWP); this state will serve as a probe and can be described by the polarization qubit  $|\Psi_{pr}\rangle = \frac{1}{\sqrt{2}}(|H\rangle + |V\rangle)$ . The preparation of the spatial mode or pointer consists of the generation of an angular mode (ANG)  $f(\phi) \propto \exp(-\phi^2/2\eta_\phi^2)$ , which is a Gaussian-apodized angular slit of width  $\eta_\phi$ . This is shaped by impressing amplitude and phase information onto the beam by means of modulation of the blaze parameters on a spatial light modulator (SLM), used together with a 4f optical system containing a spatial filter in the Fourier plane [35]. The advantages that pointer states carrying OAM provide over Gaussian pointer states have been studied [36]. The beam is injected into a Sagnac interferometer, where the horizontally and vertically polarized components of the beam circulate in opposite directions. The dove prism (DP) is rotated by a small angle  $\Delta\phi/4$  with respect to the plane of the interferometer, which causes the two counter-propagating beams to be

rotated by an amount of  $\pm\Delta\phi/2$  in opposite directions. This setup enables a coupling between the polarization, marked by the two counter propagating beams, and the transverse azimuthal DoF. In the next step we use two quarter-wave plates (QWP) and a HWP to induce a geometric phase between the two circulating beams in the interferometer, permitting the existence of complex WVs [37]. Finally, the post-selection is carried out by setting the angle of a polarizer almost orthogonal with respect to the angle of the polarizer used in the pre-selection. At this stage, a full characterization of the complex wavefunction in the transverse angular basis and the conjugate basis of OAM reveals information about the real and the imaginary part of the WV, respectively.

The interaction in our experiment can be described by the spin-orbit interaction Hamiltonian  $\hat{H}_{SO} = \mu\hat{\sigma}\hat{\ell}_z$  and a Hamiltonian that describes the action of the wave plates  $\hat{H}_g = \delta\hat{\sigma}$ , where  $\hat{\sigma}$  is the Pauli operator defined by  $\hat{\sigma} \equiv |H\rangle\langle H| - |V\rangle\langle V|$ ,  $\frac{\Delta\phi}{2} = \mu\Delta t$ ,  $(\frac{\theta_H}{2} - \frac{\pi}{2}) = \delta\Delta t$  and  $\frac{\theta_H}{2}$  is the induced geometric phase. Our state at the input of the interferometer has the following form  $|\Psi_i\rangle = |\Psi_{pr}\rangle |f(\phi)\rangle$ . The interaction which occurs in the DP couples the two DoFs as follows:

$$\begin{aligned} |\Psi_f\rangle &= e^{-i\frac{\Delta\phi}{2}\hat{\sigma}\hat{\ell}_z} e^{-i\hat{\sigma}(\frac{\theta_H}{2} - \frac{\pi}{2})} |\Psi_i\rangle \\ &= \frac{1}{\sqrt{2}} \left( e^{-i\frac{\theta}{2}} |H\rangle |f(\phi - \Delta\phi/2)\rangle + e^{i\frac{\theta}{2}} |V\rangle |f(\phi + \Delta\phi/2)\rangle \right), \end{aligned} \quad (1)$$

where  $\hat{\ell}_z$  act as the generator of rotations and is proportional to the angular momentum operator projected along the optical axis  $\hat{L}_z = \hbar\hat{\ell}_z$ , and  $\theta$  equals  $\theta_H - \pi$ . As demonstrated by Eq. 1, the weak coupling creates entanglement between probe and pointer. It should be noted

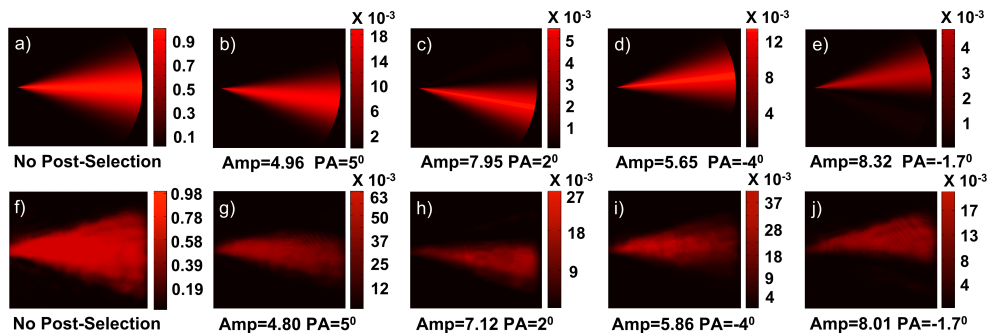


FIG. 2: Amplification of angular displacements using real weak values. a) – e) show simulations of our scheme for  $\Delta\phi = 1.2^\circ$ , different post-selection angles (PA) and amplification factors (Amp). f) – j) show experimental evidence of our protocol under the same conditions.

that since the probe and the pointer are different DoFs of a single beam rather than separate systems or particles, then this is an example of classical entanglement and thus can be described classically [38, 39]. Because of this, most traditional weak measurement experiments, such as those described in Refs. [2, 4, 5, 7–10, 36], are classically explainable. This also demonstrates what is required to perform a non-classical weak measurement experiment. We have chosen to use the mature language of weak measurement theory, since it provides a simpler description and the results readily apply to a wider range of phenomena including non-classical systems.

The post-selection is performed by projecting the perturbed state into  $|\Phi_{ps}\rangle = \sin(\frac{\gamma}{2} - \frac{\pi}{4})|H\rangle + \cos(\frac{\gamma}{2} - \frac{\pi}{4})|V\rangle$ , where  $\gamma$  is controlled by the polarizer. The post-selection collapses the polarization state of the probe and causes a shift in the angular position and the OAM spectrum of the pointer that can be described as

$$|\Psi_p\rangle = |\Phi_{ps}\rangle \langle \Phi_{ps} | \Psi_f \rangle \approx |\Phi_{ps}\rangle |f(\phi - \sigma_w \Delta\phi/2)\rangle. \quad (2)$$

Here,  $\sigma_w$  is the complex WV given by

$$\sigma_w \equiv \frac{\langle \Phi_{ps} | \hat{\sigma} | \Psi_{fpr} \rangle}{\langle \Phi_{ps} | \Psi_{fpr} \rangle} \quad (3)$$

$|\Psi_{fpr}\rangle$  is defined as  $\frac{1}{\sqrt{2}}(e^{-i\frac{\theta}{2}}|H\rangle + e^{i\frac{\theta}{2}}|V\rangle)$ . If the induced phase  $\theta$  and polarizer selection angle  $\gamma/2$  are small, the WV can be approximated as [40]

$$\sigma_w \approx -\frac{2\gamma}{\gamma^2 + \theta^2} + i\frac{2\theta}{\gamma^2 + \theta^2}. \quad (4)$$

The post-selected state described in Eq. 2 shows a change in angle as  $\phi \rightarrow \phi - \sigma_w \Delta\phi/2$ . If  $\sigma_w$  is real, which will be the case for  $\theta = 0$ , then this leads to the rotation of the pointer by the amount  $\sigma_w$ . However if  $\sigma_w$  is complex then

$$\begin{aligned} f(\phi - \sigma_w \Delta\phi/2) &= e^{-(\phi - \sigma_w \Delta\phi/2)^2 / 2\eta_\phi^2} \\ &\propto e^{-(\phi - \Re(\sigma_w) \Delta\phi/2)^2 / 2\eta_\phi^2} e^{i\phi \Im(\sigma_w) \Delta\phi/2\eta_\phi^2} \\ &= e^{-(\phi - \Delta\langle\phi\rangle)^2 / 2\eta_\phi^2} e^{i\phi \Delta\langle\ell\rangle}, \end{aligned} \quad (5)$$

where  $\Delta\langle\phi\rangle = \Re(\sigma_w) \Delta\phi/2$  sets the amount of the pointer's rotation. In addition, the pointer experiences a shift in its OAM spectrum that equals  $\Delta\langle\ell\rangle = \Im(\sigma_w) \Delta\phi/2\eta_\phi^2$ . We have used the angular representation of the spatial mode of the photons, and utilized the Fourier relation between the conjugate pairs of azimuthal angle and angular momentum. Alternatively, the same results can be derived by using the commutation relation between angular position and OAM operators, which is given by  $[\phi, \hat{L}_z] = i\hbar(1 - 2\pi P(\phi))$  where  $P(\phi)$  represents the angular probability at the boundary of the angle range [41]. The shift in the OAM spectrum can be understood as a form of interaction between spin angular momentum (SAM) and OAM. This interesting optical effect is a consequence of the polarization-sensitive nature of the interactions in the interferometer, and should not be confused with the standard spin-orbit coupling in the vector beams where both the SAM and OAM are directed along the same axis [42].

In the experiment we use a 3 mW He-Ne laser (632.8 nm) which is coupled to a single-mode fiber (SMF) and then expanded to a spot size of 1.8 cm. The central part of the beam homogeneously illuminates the display of the SLM that has an active area of  $9.3 \times 7\text{mm}^2$ . Due to the reflectance of the SLM and the efficiency of the encoded diffractive grating on it, the power drops to 470 nW once an ANG mode of width  $\eta_\phi = 13.7^\circ$  is generated. The DP in the Sagnac interferometer is rotated by  $0.3^\circ$ , this angle is determined by measuring a relative rotation of  $1.2^\circ$  between two identical ANG modes propagating in the opposite directions. The induced displacement  $\Delta\phi$ , is chosen to be much smaller than the width of the ANG mode, in order to guarantee the conditions for the weak perturbation. The post-selection polarizer is set to an angle  $\gamma/2$ , with respect to the polarization state of the pre-selected state. For this part, we have set  $\theta$  to zero.

Since our interest is in the amplification of the weak-value, the angle  $\gamma/2$  is set to a small number. The post-selection polarizer forces the two ANG modes to coherently interfere, producing another ANG mode which is

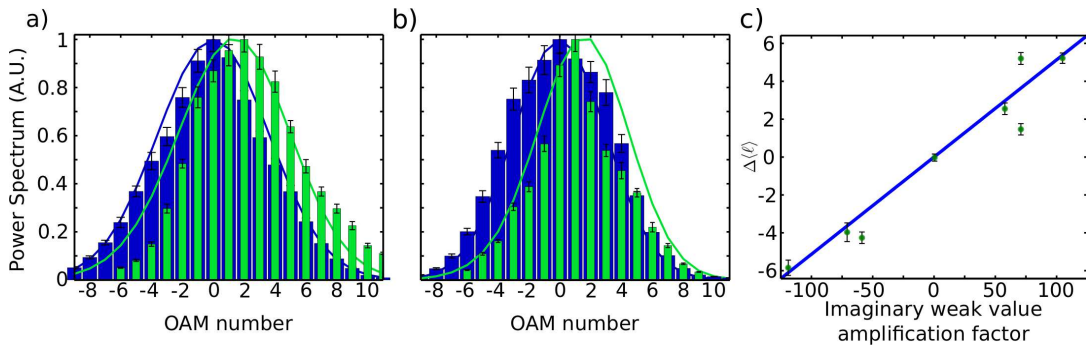


FIG. 3: Measured OAM power spectra of  $|\Psi_p\rangle$  without post-selection (blue) and with post-selection (green) demonstrating the shift in  $\langle\ell\rangle$  due to  $\Im(\sigma_w)$  for a)  $\eta_\phi = 11.4^\circ$ ,  $\gamma/2 = 6^\circ$  and b)  $\eta_\phi = 13.7^\circ$  and  $\gamma/2 = 5^\circ$ . The angle  $\theta/2$  equals  $5^\circ$  for all the cases. Histograms represent measured data, while lines represent theoretically predicted shifts. c) OAM centroid shift  $\Delta\langle\ell\rangle$  for various measured OAM power spectra plotted against the imaginary WV amplification factor,  $\Im(\sigma_w)/2\eta_\phi^2$ . Dots represent data, while the line is the theoretical linear curve predicted by Eq. 5.

rotated due to the azimuthal Gaussian intensity distribution impressed in the ANG [43]. Such rotation is proportional to the angular displacement  $\Delta\phi$  and the real part of the WV  $\Re(\sigma_w)$ . Since the WV can take values larger than one, this scheme allows the amplification of small rotations. However, as  $\Re(\sigma_w)$  is increased more photons are lost as shown for different post-selection angles (PA) in Fig. 2a–e. In order to detect this effect, a CCD camera is placed after the polarizer. This is equivalent to measuring the expected value of the angular position in the state  $|\Psi_p\rangle$ . As shown in Fig. 2f–j, the measured power is in the range of 10–30 nW, however these images were taken using long exposure times. As can be seen in Fig. 2, an aggressive post-selection leads to a larger rotation. The amplification factor (Amp) is defined as the ratio between the angular position of the post-selected mode  $\Delta\langle\phi\rangle$  and  $\Delta\phi$ . This is equal to  $\Re(\sigma_w)/2$ . Both  $\Delta\langle\phi\rangle$  and  $\Delta\phi$  were determined by using centroid measurements. The amplification limit is given by the extinction ratio of the polarizer and the magnitude of the weak perturbation or the angle of post-selection. Larger amplifications can be measured if the width of ANG is increased and the post-selection angle is decreased.

The imaginary part of the WV can be determined by analyzing the shift of the OAM spectrum of the ANG. We have chosen the rotation angle of the DP to be approximately  $0.4^\circ$  and we have tried different angular widths for the input state. In order to allow  $\Im(\sigma_w)$  to be nonzero, the phase  $\theta$  must also be nonzero. This is done by inducing a geometric phase between the polarization states  $|H\rangle$  and  $|V\rangle$ . This phase is created using three rotatable wave plates as shown in Fig. 1. The angle of the QWPs is set to  $\pi/4$  and the HWP is rotated by a small angle [37]. We have set the HWP to an angle such that  $\theta/2 = 5^\circ$  and tried several different post-selection angles for the polarizer. Measurement of the OAM spectrum associated with a beam can be done using a wide variety of techniques [44–47]. We measured the OAM using a

series of projective measurements for various values of  $\ell$ . Using a similar procedure as was used for generating the angular slits, a hologram was impressed onto a SLM and then a Fourier transforming lens and a spatial filtering from a SMF couples photons to an APD which allows measurement at single photon levels [48].

We summed the counts during a 0.2 second window and averaged it for 30 measurements for each projection over different OAM modes. This procedure was repeated for each mode and the reconstructed spectra are shown in Fig. 3a–b. The error bars represent the standard deviation over the ensemble of 30 measurements. The spectrum is broader for angular modes with narrower widths due to uncertainty relation between angular position and OAM [41]. As predicted by Eq. 5, and shown in Fig. 3, the larger amplifications are obtained for angular modes with narrow widths. However, such narrow ANG modes have physically smaller cross sections and hence carry proportionally less power. Each OAM power spectra was fitted using a weighted least-squares minimization to a shifted Gaussian function. The mean values are plotting in Fig. 3c along with error bars representing the  $3\sigma$  confidence interval. By exploiting the measurement process we have amplified small rotations by a magnitude of 100 without using high OAM nor entanglement.

Recently, there has been research casting doubt on the sensitivity of measurements based on WVA [49]. However, it has been shown that in the presence of technical noise WVs, and more specifically imaginary WVs, outperform traditional measurements [50]. Therefore, our experiment can be potentially useful for sensitive measurement of small rotation in real world scenarios. A quantitative analysis of the sensitivity of our scheme can be done by using the Fisher information metric. However, such quantitative comparison is outside the scope of the current work and will be the subject of a future study.

We have made the first step towards the study of WVA

in the azimuthal DoF. This has been approached by describing the mechanisms that lead to a shift in the angular position and OAM of an optical beam. The OAM spectrum is shifted as a consequence of the breakup in the polarization symmetry, realized by a differential geometric phase. Furthermore, we have implemented the first realization of WVA in the angular position and OAM bases. The results presented here provide a proof-of-principle demonstration of the scope of WVA in this DOF. We believe that our protocol opens the possibility for new schemes in optical metrology. In addition, our approach shows an alternative fashion to study the exchange between SAM and OAM in optical systems.

We acknowledge discussions with J. Vornehm, G. Viza, J. Martinez-Rincon, J. C. Howell and E. Karimi. This work was supported by DARPA, CERC and CONACyT.

---

\* Electronic address: omar.maganaloaiza@rochester.edu

† Electronic address: mirhosse@optics.rochester.edu

‡ Electronic address: brandon.rodenburg@gmail.com

- [1] Y. Aharonov, D. Albert, and L. Vaidman, *Phys. Rev. Lett.* **60**, 1351 (1988).
- [2] P. Dixon, D. Starling, A. Jordan, and J. Howell, *Phys. Rev. Lett.* **102**, 173601 (2009).
- [3] O. Hosten and P. Kwiat, *Science* **319**, 787 (2008).
- [4] N. Brunner and C. Simon, *Phys. Rev. Lett.* **105**, 010405 (2010).
- [5] X.-Y. Xu, Y. Kedem, K. Sun, L. Vaidman, C.-F. Li, and G.-C. Guo, *Phys. Rev. Lett.* **111**, 033604 (2013).
- [6] G. Strübi and C. Bruder, *Phys. Rev. Lett.* **110**, 083605 (2013).
- [7] J. S. Lundeen, B. Sutherland, A. Patel, C. Stewart, and C. Bamber, *Nature* **474**, 188 (2011).
- [8] J. Z. Salvail, M. Agnew, A. S. Johnson, E. Bolduc, J. Leach, and R. W. Boyd, *Nature Photonics* **7**, 316 (2013).
- [9] M. Malik, M. Mirhosseini, M. P. J. Lavery, J. Leach, M. J. Padgett, and R. W. Boyd, *Nature Communications* **5**, 4115 (2014).
- [10] H. Kobayashi, K. Nonaka, and Y. Shikano, arXiv:1311.3357 (2013).
- [11] A. Feizpour, X. Xing, and A. M. Steinberg, *Phys. Rev. Lett.* **107**, 133603 (2011).
- [12] S. Kocsis, B. Braverman, S. Ravets, M. J. Stevens, R. P. Mirin, L. K. Shalm, and A. M. Steinberg, *Science* **332**, 1170 (2011).
- [13] Y. Aharonov, A. Botero, S. Popescu, and B. Reznik, *Phys. Lett. A* **301**, 130 (2002).
- [14] L. J. Salazar-Serrano, D. Janner, N. Brunner, V. Pruneri, and J. P. Torres, *Phys. Rev. A* **89**, 012126 (2014).
- [15] H. F. Hofmann, *Phys. Rev. A* **83**, 022106 (2011).
- [16] V. Giovannetti, S. Lloyd, and L. Maccone, *Nature Photonics* **5**, 222 (2011).
- [17] N. Thomas-Peter, B. J. Smith, A. Datta, L. Zhang, U. Dorner, and I. A. Walmsley, *Phys. Rev. Lett.* **107**, 113603 (2011).
- [18] H. Shin, O. S. Magaña-Loaiza, M. Malik, M. N. O’Sullivan, and R. W. Boyd, *Opt. Express* **21**, 2816 (2013).
- [19] B. L. Higgins, D. W. Berry, S. D. Bartlett, H. M. Wiseman, and P. G. J. Nature **450**, 393 (2007).
- [20] L. H. Thomas, *Nature* **117**, 514 (1926).
- [21] T. L. Gustavson, P. Bouyer, and M. A. Kasevich, *Phys. Rev. Lett.* **78**, 2046 (1997).
- [22] J. K. Stockton, K. Takase, and M. A. Kasevich, *Phys. Rev. Lett.* **107**, 133001 (2011).
- [23] L. Allen, M. W. Beijersbergen, R. J. C. Spreeuw, and J. P. Woerdman, *Phys. Rev. A* **45**, 8185 (1992).
- [24] M. Padgett and R. Bowman, *Nature Photonics* **5**, 343 (2011).
- [25] J. Courtial, D. A. Robertson, K. Dholakia, L. Allen, and M. J. Padgett, *Phys. Rev. Lett.* **81**, 4828 (1998).
- [26] M. P. J. Lavery, F. C. Speirits, S. M. Barnett, and M. J. Padgett, *Science* **341**, 537 (2013).
- [27] C. Rosales-Guzmán, N. Hermosa, A. Belmonte, and J. P. Torres, *Scientific Reports* **3** (2013).
- [28] V. D’Ambrosio, N. Spagnolo, L. Del Re, S. Slussarenko, Y. Li, L. C. Kwek, L. Marrucci, S. P. Walborn, L. Aolita, and F. Sciarrino, *Nature Communications* **4**, 1 (2013).
- [29] R. Fickler, R. Lapkiewicz, W. N. Plick, M. Krenn, C. Schaeff, S. Ramelow, and A. Zeilinger, *Science* **338**, 640 (2012).
- [30] A. K. Jha, G. S. Agarwal, and R. W. Boyd, *Phys. Rev. A* **83**, 053829 (2011).
- [31] N. Uribe-Patarroyo, A. Fraine, D. S. Simon, O. Minaeva, and A. V. Sergienko, *Phys. Rev. Lett.* **110**, 043601 (2013).
- [32] Y. Gorodetski, K. Y. Bliokh, B. Stein, C. Genet, N. Shitrit, V. Kleiner, E. Hasman, and T. W. Ebbesen, *Phys. Rev. Lett.* **109**, 013901 (2012).
- [33] H. Luo, S. Wen, W. Shu, Z. Tang, Y. Zou, and D. Fan, *Phys. Rev. A* **78**, 033805 (2008).
- [34] S. Franke-Arnold, G. Gibson, R. W. Boyd, and M. J. Padgett, *Science* **333**, 65 (2011).
- [35] J. A. Davis, D. M. Cottrell, J. Campos, M. J. Yzuel, and I. Moreno, *Appl. Opt.* **38**, 5004 (1999).
- [36] G. Puentes, N. Hermosa, and J. P. Torres, *Phys. Rev. Lett.* **109**, 040401 (2012).
- [37] O. S. Magaña Loaiza, M. Mirhosseini, B. Rodenburg, and R. W. Boyd, More detailed information is provided in the supplementary Information. (Section I.).
- [38] X. F. Qian and J. H. Eberly, *Opt. Lett.* **36**, 4110 (2011).
- [39] K. H. Kagalwala, G. Di Giuseppe, A. F. Abouraddy, and B. E. A. Saleh, *Nature Photonics* **7**, 72 (2012).
- [40] O. S. Magaña Loaiza, M. Mirhosseini, B. Rodenburg, and R. W. Boyd, More detailed information is provided in the supplementary Information. (Section II.).
- [41] S. Franke-Arnold, S. M. Barnett, E. Yao, J. Leach, J. Courtial, and M. Padgett, *New J. Phys.* **6**, 103 (2004).
- [42] E. Nagali, F. Sciarrino, F. De Martini, L. Marrucci, B. Piccirillo, E. Karimi, and E. Santamato, *Phys. Rev. Lett.* **103**, 013601 (2009).
- [43] N. Ritchie, J. Story, and R. Hulet, *Phys. Rev. Lett.* **66**, 1107 (1991).
- [44] A. Mair, A. Vaziri, G. Weihs, and A. Zeilinger, *Nature* **412**, 313 (2001).
- [45] J. Leach, M. J. Padgett, S. M. Barnett, S. Franke-Arnold, and J. Courtial, *Phys. Rev. Lett.* **88**, 257901 (2002).
- [46] G. C. G. Berkhout, M. P. J. Lavery, J. Courtial, M. W. Beijersbergen, and M. J. Padgett, *Phys. Rev. Lett.* **105**, 153601 (2010).
- [47] M. Mirhosseini, M. Malik, Z. Shi, and R. W. Boyd, *Nature Communications* **4**, 2781 (2013).

- [48] O. S. Magaña Loaiza, M. Mirhosseini, B. Rodenburg, and R. W. Boyd, More detailed information is provided in the supplementary Information. (Section III.).  
 [49] C. Ferrie and J. Combes, Phys. Rev. Lett. **112**, 040406

- (2014).  
 [50] A. N. Jordan, J. Martínez-Rincón, and J. C. Howell, Phys. Rev. X **4**, 011031 (2014).

---

## Supplementary information

The main purpose of this document is to provide more detailed information about the design of our experimental setup and recast its functionality in terms of the “weak measurement” formalism. In addition, we describe the scheme employed to measure the OAM spectrum of a beam of light.

### I. Sagnac interferometer

We use a Sagnac interferometer composed of a polarized beam splitter (PBS), a Dove prism (DP) and a series of rotatable plates. In this first section, we will describe the role of the DP and how we use the rotatable plates to introduce geometric phases.

As mentioned in the article, a spatial mode  $|f(\phi)\rangle$  is diagonally polarized and injected into the input port of the interferometer, and the polarization information is described by the state  $|\Psi_{pr}\rangle$ . Therefore we can describe the initial state as  $|f(\phi)\rangle|\Psi_{pr}\rangle$ . The beam is split into two polarization components that circulate in opposite directions within the interferometer. The role of the DP is to rotate the beam. When the DP is rotated by an angle of  $\Delta\phi/4$  about its optical axis, the transmitted beam suffers a rotation of  $\pm\Delta\phi/2$ , where the sign is determined by the propagation direction of the beam. In our experiment, the DP couples the polarization degree of freedom (DoF) to the spatial DoF of the beam. The action of the DP inside the polarized Sagnac interferometer is described as follows:

$$\begin{aligned} |\Psi_{pr}\rangle|f(\phi)\rangle &\rightarrow [Prism]Dove \frac{1}{\sqrt{2}}(\mathbf{R}(-\phi/2)|f(\phi)\rangle|H\rangle + \mathbf{R}(\phi/2)|f(\phi)\rangle|V\rangle) \\ &= \frac{1}{\sqrt{2}}|f(\phi - \Delta\phi/2)\rangle|H\rangle + |f(\phi + \Delta\phi/2)\rangle|V\rangle, \end{aligned} \quad (S1)$$

where the operator  $\mathbf{R}(\phi/2)$  is given by  $e^{i\hat{\ell}\Delta\phi/2}$ .  $\hat{\ell}$  is the generator of rotations and is proportional to the operator representing angular momentum along the optical axis.

The role of the wave plates is to induce a geometric phase, which we will describe using the Jones matrix formalism. Here the polarization states are defined as:

$$|H\rangle = \begin{bmatrix} 1 \\ 0 \end{bmatrix} \quad \text{and} \quad |V\rangle = \begin{bmatrix} 0 \\ 1 \end{bmatrix}. \quad (S2)$$

The action of the quarter-wave plate **QWP** and half-wave plate **HWP** are described by the following matrices,

$$\begin{aligned} \mathbf{QWP} = & \\ & \begin{bmatrix} e^{i\phi_{x1}}\cos^2(\theta_Q) + e^{i\phi_{y1}}\sin^2(\theta_Q) & (e^{i\phi_{x1}} - e^{i\phi_{y1}})\cos(\theta_Q)\sin(\theta_Q) \\ (e^{i\phi_{x1}} - e^{i\phi_{y1}})\cos(\theta_Q)\sin(\theta_Q) & e^{i\phi_{x1}}\sin^2(\theta_Q) + e^{i\phi_{y1}}\cos^2(\theta_Q) \end{bmatrix}, \end{aligned} \quad (S3)$$

and

$$\mathbf{HWP} = \begin{bmatrix} \cos(2\theta_H) & \sin(2\theta_H) \\ \sin(2\theta_H) & -\cos(2\theta_H) \end{bmatrix}. \quad (S4)$$

$\theta_Q$  represents the orientation of the fast axis of the QWP, with respect to the x-axis, and  $\theta_H$  represents the orientation of the HWP. The value  $\phi_y - \phi_x$  determines the induced retardation phase between the two components of the electric field. For a QWP this number is equal to  $\pi/2$ .

The configuration used to induce the geometric phase consists of a HWP sandwiched between two QWPs. The angle  $\theta_Q$  was set to  $\pi/4$  whereas the angle of the HWP,  $\theta_H$ , was set to  $\theta_H/4$ . Thus the Eqs. S3–S4 become

$$\mathbf{QWP}_{\pm} = \begin{bmatrix} \frac{1}{2} + \frac{i}{2} & \pm(\frac{1}{2} - \frac{i}{2}) \\ \pm(\frac{1}{2} - \frac{i}{2}) & \frac{1}{2} + \frac{i}{2} \end{bmatrix}, \quad (S5)$$

and

$$\mathbf{HWP}_{\pm} = \begin{bmatrix} \cos(\theta_H/2) & \pm \sin(\theta_H/2) \\ \pm \sin(\theta_H/2) & -\cos(\theta_H/2) \end{bmatrix}. \quad (\text{S6})$$

Different orientation angles have to be considered for each of the counter-propagating beams. Here we use positive and negative values for the horizontally and negative polarized beams respectively. The transformation suffered by each beam is thus given by

$$\begin{aligned} |H^g\rangle &= \mathbf{QWP}_+ \cdot \mathbf{HWP}_+ \cdot \mathbf{QWP}_+ |H\rangle \\ &= e^{-i(\theta_H/2 - \pi/2)} |H\rangle, \end{aligned} \quad (\text{S7})$$

and

$$\begin{aligned} |V^g\rangle &= \mathbf{QWP}_- \cdot \mathbf{HWP}_- \cdot \mathbf{QWP}_- |V\rangle \\ &= e^{i(\theta_H/2 - \pi/2)} |V\rangle. \end{aligned} \quad (\text{S8})$$

As can be seen, the net effect is the acquisition of a phase given by  $\pm(\theta_H/2 - \pi/2)$ , which is the geometric phase.

## II. The action of sagnac interferometer in terms of the weak measurement formalism

In this section we describe our weak measurement protocol. The action of the interferometer is described by the following interaction Hamiltonian:

$$\hat{H}_T = \hat{H}_g + \hat{H}_{SO}. \quad (\text{S9})$$

The Hamiltonian  $\hat{H}_g$  describes the role of the three wave plates. It is given by  $\delta\hat{\sigma}$ . The spin-orbit interaction caused by the DP is described by  $\hat{H}_{SO}$ , which is given by a Hamiltonian of the form  $\mu\hat{\sigma}\hat{\ell}$ , where  $\hat{\sigma}$  is the Pauli operator defined as  $|H\rangle\langle H| - |V\rangle\langle V|$ ,  $(\theta_H/2 - \pi/2) = \delta\Delta t$  and  $\Delta\phi/2 = \mu\Delta t$ . Given this, the evolution of the initial state  $|\Psi_i\rangle = |\Psi_{pr}\rangle |f(\phi)\rangle$  to a final state  $|\Psi_f\rangle$  is given as

$$\begin{aligned} |\Psi_f\rangle &= e^{-i\hat{H}_T\Delta t} |\Psi_{pr}\rangle |f(\phi)\rangle \\ &= e^{-i\hat{H}_g\Delta t} \left[ \frac{1}{\sqrt{2}}(|H\rangle + |V\rangle) |f(\phi)\rangle \right. \\ &\quad \left. - i\frac{\Delta\phi}{2\sqrt{2}}(|H\rangle\langle H| - |V\rangle\langle V|)(|H\rangle + |V\rangle)\hat{\ell} |f(\phi)\rangle + \dots \right], \end{aligned} \quad (\text{S10})$$

This expression can be rewritten as

$$\begin{aligned} |\Psi_f\rangle &= \\ &= \frac{e^{-i\hat{H}_g\Delta t}}{\sqrt{2}} \left[ |H\rangle (1 - i\frac{\Delta\phi}{2}\hat{\ell} + \dots) |f(\phi)\rangle + |V\rangle (1 + i\frac{\Delta\phi}{2}\hat{\ell} + \dots) |f(\phi)\rangle \right]. \end{aligned} \quad (\text{S11})$$

The expression in parenthesis is a translation operator in the azimuthal degree of freedom which leads to the state

$$|\Psi_f\rangle = \frac{e^{-i\hat{H}_g\Delta t}}{\sqrt{2}} [|H\rangle |f(\phi - \Delta\phi/2)\rangle + |V\rangle |f(\phi + \Delta\phi/2)\rangle]. \quad (\text{S12})$$

The action of  $\hat{H}_g$  leads to the state

$$\begin{aligned} |\Psi_f\rangle &= \frac{1}{\sqrt{2}} [e^{-i(\theta_H/2 - \pi/2)} |H\rangle |f(\phi - \Delta\phi/2)\rangle \\ &\quad + e^{i(\theta_H/2 - \pi/2)} |V\rangle |f(\phi + \Delta\phi/2)\rangle]. \end{aligned} \quad (\text{S13})$$

The state above describes our experiment just before post-selection by the polarizer is performed.  $|\Psi_f\rangle$  is the state of the photons emerging from the output port of the polarized beam splitter. The post-selection process is described by the projection operator  $|\Phi_{ps}\rangle\langle\Phi_{ps}|$  which gives the post-selected state

$$\begin{aligned} |\Psi_p\rangle &= |\Phi_{ps}\rangle\langle\Phi_{ps}|\Psi_f\rangle \\ &= [\langle\Phi_{ps}|e^{-i\hat{H}_g\Delta t}|\Psi_{pr}\rangle|f(\phi)\rangle \\ &\quad - i\frac{\Delta\phi}{2}\langle\Phi_{ps}|e^{-i\hat{H}_g\Delta t}\hat{\sigma}|\Psi_{pr}\rangle\hat{\ell}|f(\phi)\rangle + \dots]|\Phi_{ps}\rangle. \end{aligned} \quad (\text{S14})$$

This expression can be approximated to the first order and then normalized:

$$|\Psi_p\rangle \approx \left( |f(\phi)\rangle - i\frac{\Delta\phi}{2}\frac{\langle\Phi_{ps}|e^{-i\hat{H}_g\Delta t}\hat{\sigma}|\Psi_{pr}\rangle}{\langle\Phi_{ps}|e^{-i\hat{H}_g\Delta t}|\Psi_{pr}\rangle}\hat{\ell}|f(\phi)\rangle \right) |\Phi_{ps}\rangle \quad (\text{S15})$$

Since  $\hat{\sigma}$  commutes with  $e^{-i\hat{H}_g\Delta t}$

$$|\Psi_p\rangle = \left( |f(\phi)\rangle - i\frac{\Delta\phi}{2}\frac{\langle\Phi_{ps}|\hat{\sigma}|\Psi_{fpr}\rangle}{\langle\Phi_{ps}|\Psi_{fpr}\rangle}\hat{\ell}|f(\phi)\rangle \right) |\Phi_{ps}\rangle, \quad (\text{S16})$$

where  $|\Psi_{fpr}\rangle \equiv e^{-i\hat{H}_g\Delta t}|\Psi_{pr}\rangle$ . Defining the weak value of  $\hat{\sigma}$  as

$$\sigma_w \equiv \frac{\langle\Phi_{ps}|\hat{\sigma}|\Psi_{fpr}\rangle}{\langle\Phi_{ps}|\Psi_{fpr}\rangle}, \quad (\text{S17})$$

then the total effect of the post-selection can be written as

$$|\Psi_p\rangle = |f(\phi - \sigma_w\Delta\phi/2)\rangle |\Phi_{ps}\rangle. \quad (\text{S18})$$

The weak value of the polarization operator can be determined by using the following form for the states:

$$\begin{aligned} |\Psi_{fpr}\rangle &= \frac{1}{\sqrt{2}} \left( e^{-i(\theta_H/2 - \pi/2)} |H\rangle + e^{i(\theta_H/2 - \pi/2)} |V\rangle \right) \\ |\Phi_{ps}\rangle &= \sin(\gamma/2 - \pi/4) |H\rangle + \cos(\gamma/2 - \pi/4) |V\rangle. \end{aligned} \quad (\text{S19})$$

It is worth noting that  $|\Phi_{ps}\rangle$  is almost orthogonal with respect to  $|\Psi_{pr}\rangle$ . Using the above states the weak value becomes

$$\sigma_w = \frac{\tan(\gamma/2 - \pi/4) e^{-i(\theta_H - \pi)} - 1}{\tan(\gamma/2 - \pi/4) e^{-i(\theta_H - \pi)} + 1}. \quad (\text{S20})$$

For simplicity we can define the angle  $\theta_H - \pi$  as  $\theta$ . If we assume that  $\gamma/2$  and  $\theta$  are very small, corresponding to the weak measurement regime, then this expression becomes

$$\begin{aligned} \sigma_w &= \frac{e^{-i\theta} \frac{\tan(\gamma/2) - \tan(\pi/4)}{1 + \tan(\gamma/2) \tan(\pi/4)} - 1}{e^{-i\theta} \frac{\tan(\gamma/2) - \tan(\pi/4)}{1 + \tan(\gamma/2) \tan(\pi/4)} + 1} \\ &\approx \frac{(1 - i\theta) \frac{\gamma - 2}{2 + \gamma} - 1}{(1 - i\theta) \frac{\gamma - 2}{2 + \gamma} + 1} \\ &= \frac{\gamma - 2 - i\theta\gamma + 2i\theta - \gamma - 2}{\gamma - 2 - \theta\gamma + 2i\theta + \gamma + 2} \\ &\approx \frac{-2}{\gamma + i\theta} = -2 \frac{\gamma}{\gamma^2 + \theta^2} + 2 \frac{i\theta}{\gamma^2 + \theta^2}. \end{aligned} \quad (\text{S21})$$



### III. Projective measurements

In this section we describe a simple form of measuring the OAM power spectrum of an ensemble of photons. The technique employed is known as projection measurements. Here a spatial mode (in our case an angular mode  $f(\mathbf{r})$ ), which can be written in terms of the modal expansion  $\sum_{\ell} a_{\ell} e^{i\ell\phi}$ , is imaged onto a SLM that transforms the field in the first diffracted order to:

$$f(\mathbf{r})e^{-i\ell\phi}. \quad (\text{S22})$$

A Fourier transforming lens takes the field above to

$$f_{\ell}(\boldsymbol{\rho}) = \mathcal{F}[f(\mathbf{r})e^{-i\ell\phi}], \quad (\text{S23})$$

which is spatially filtered using a SMF coupled to an avalanche photodiode (APD) which allows measurement at single photon levels. The coupling efficiency into the fiber,  $\eta_{\ell}$  is given by

$$\eta_{\ell} \propto \left| \int f_{\ell}(\boldsymbol{\rho}) e^{-\frac{\rho^2}{2\eta^2}} d^2\boldsymbol{\rho} \right|^2, \quad (\text{S24})$$

where  $\eta$  is the Gaussian width of the fiber mode. Assuming features of  $f_{\ell}$  to be of size scale larger than  $\eta$ , this filtering function becomes

$$\eta_{\ell} \approx \left| \int f_{\ell}(0) e^{-\frac{\rho^2}{2\eta^2}} d^2\boldsymbol{\rho} \right|^2 \propto |f_{\ell}(0)|^2 = \left| \sum_{\ell'} \int a_{\ell'} e^{i(\ell' - \ell)\phi} d^2\mathbf{r} \right|^2 = |a_{\ell}|^2, \quad (\text{S25})$$

permitting us to obtain the OAM power spectrum component  $|a_{\ell}|^2$ . This process is repeated for the different modes contained in the spatial mode. The efficiency of this technique for different spatial modes, such as radial modes, has been studied in reference [S1].

---

\* Electronic address: omar.maganaloaiza@rochester.edu

† Electronic address: mirhosse@optics.rochester.edu

‡ Electronic address: brandon.rodenburg@gmail.com

[S1] H. Qassim, F. M. Miatto, J. P. Torres, M. J. Padgett, E. Karimi, and R. W. Boyd, e-print arXiv:1401.3512 (2013).